Supercapacitor to Provide Ancillary Services

Preprint

V. Gevorgian,[1] E. Muljadi,[1] Y. Luo,[2]
M. Mohanpurkar,[2] R. Hovsapian,[2] and
V. Koritarov[3]

[1] *National Renewable Energy Laboratory*
[2] *Idaho National Laboratory*
[3] *Argonne National Laboratory*

Presented at the 2017 IEEE Energy Conversion Congress and Exhibition (IEEE ECCE)
Cincinnati, Ohio
October 1–5, 2017

NREL is a national laboratory of the U.S. Department of Energy
Office of Energy Efficiency & Renewable Energy
Operated by the Alliance for Sustainable Energy, LLC

This report is available at no cost from the National Renewable Energy Laboratory (NREL) at www.nrel.gov/publications.

Conference Paper
NREL/CP-5D00-68740
October 2017

Contract No. DE-AC36-08GO28308

NOTICE

This report is available at no cost from the National Renewable Energy Laboratory (NREL) at www.nrel.gov/publications.

Available electronically at SciTech Connect http:/www.osti.gov/scitech

Available for a processing fee to U.S. Department of Energy and its contractors, in paper, from:

U.S. Department of Energy
Office of Scientific and Technical Information
P.O. Box 62
Oak Ridge, TN 37831-0062
OSTI http://www.osti.gov
Phone: 865.576.8401
Fax: 865.576.5728
Email: reports@osti.gov

Available for sale to the public, in paper, from:

U.S. Department of Commerce
National Technical Information Service
5301 Shawnee Road
Alexandria, VA 22312
NTIS http://www.ntis.gov
Phone: 800.553.6847 or 703.605.6000
Fax: 703.605.6900
Email: orders@ntis.gov

Cover Photos by Dennis Schroeder: (left to right) NREL 26173, NREL 18302, NREL 19758, NREL 29642, NREL 19795.

NREL prints on paper that contains recycled content.

Supercapacitor to Provide Ancillary Services

V. Gevorgian, *Senior Member, IEEE*, E. Muljadi, *Fellow, IEEE,* Yusheng Luo, *Member, IEEE,*
M. Mohanpurkar, *Member, IEEE,* R. Hovsapian, *Member, IEEE,* V. Koritarov, *Member, IEEE*

***Abstract*—Supercapacitor technology has reached a level of maturity as a viable energy storage option available to support a modern electric power system grid; however, its application is still limited because of its energy capacity and the cost of the commercial product.**

In this paper, we demonstrate transient models of supercapacitor energy storage plants operating in coordination with run-of-the-river (ROR), doubly-fed induction generator hydropower plants (HPP) using a conceptual system control architecture. A detailed transient model of a supercapacitor energy storage device is coupled with the grid via a three-phase inverter/rectifier and bidirectional DC-DC converter. In addition, we use a version of a 14-bus IEEE test case that includes the models of the supercapacitor energy storage device, ROR HPPs, and synchronous condensers that use the rotating synchronous generators of retired coal-powered plants.

In this paper, we emphasize the control coordination among the components of the power system. The control actions must be coordinated and prioritized based on the capability, response time, the power rating, and the energy content of the components.

I. Introduction

THE increasing demand to reduce fossil-fuel consumption has led to the increased use of renewable energy resources for electricity generation [1]–[2]. Compared to traditional fossil-fueled generation, renewable energy resources emit fewer carbon-dioxide emissions, are more environmental friendly, and have lower costs of operation [3]–[4]; However, the spatiotemporal variability in renewable energy resources produces variable output power. To reduce the impact of this output variability, energy storage can serve as a reservoir to store excess generation during low-load periods and inject power back into the grid during times of high load demand [5].

Energy storage devices have diverse forms of physical realizations and operational characteristics [6]. Because of differences in physical configurations, technologies, and densities of power and energy, to implement optimal control of multiple energy storage is nontrivial [7]. Applications of energy storage devices in power systems vary widely based on system characteristics and needs [8]. A battery energy storage device is mainly used to reduce the operational cost of overall storage, which is high because of its high energy density [9]; however, because of its slow response speed, it cannot provide frequency support.

Flywheels can be considered a medium-fast response energy storage device, which is a trade-off between higher energy and power density [7]. Supercapacitors feature a fast-charging/discharging characteristic that can satisfy a power density application, but are unable to provide long-term energy storage [10-11].

II. Basic Equations

Short-term energy storage is achieved by using supercapacitors (also called ultracapacitors). Supercapacitors are electrochemical capacitors that exhibit high energy density compared to conventional capacitors (even when compared to electrolytic capacitors), reaching values of thousands of farads [11]. Their nominal voltage is relatively low, so series of connected supercapacitors are needed for higher voltage applications.

The energy, W, stored in a capacitor is directly proportional to its capacitance, C, and square of DC voltage, V, across the capacitor:

$$W = \frac{1}{2}CV^2 \qquad (1)$$

All capacitors have voltage limits. Exceeding these can cause dielectric breakdown, resulting in permanent damage. Thus, the maximum energy, W_{max}, that the capacitor can store can be calculated from the maximum allowable capacitor voltage, V_{max}. The energy capacity of a capacitor grows dramatically with the voltage because of the square rule. Therefore, higher voltage supercapacitor storage is preferred because of its energy capacity.

The charging and discharging characteristics of supercapacitor energy storage can be controlled so that constant current or constant power output can be achieved. No energy is stored in the capacitor when the DC across its terminals equals zero. The decay of capacitor voltage at constant power discharge can be calculated using the following basic capacitor equations:

$$I = C\frac{dV}{dt} \text{ and } I = \frac{P}{V} \qquad (2)$$

where I and P are the discharging current and discharging power, respectively.

After a simple mathematical transformation, the following integral equation can be derived:

$$\int VdV = \frac{1}{C}\int Pdt \qquad (3)$$

Then, the voltage decay profile vs. time at a given initial voltage, V_{max}, and discharging power, P, can be written as:

$$V(t) = \sqrt{V_{max}^2 - \frac{2Pt}{C}} \qquad (4)$$

Fig. 1 shows example voltage decay profiles for a 20-F, 1,000-V capacitor bank discharging at 1-, 2-, and 3-MW constant power, respectively. In this example, a 20-F capacitor with initial voltage of 1,000 V can potentially inject 1 MW into an electric grid for 10 s, at 2 MW for 5 s, and at 3 MW for 3.3 s.

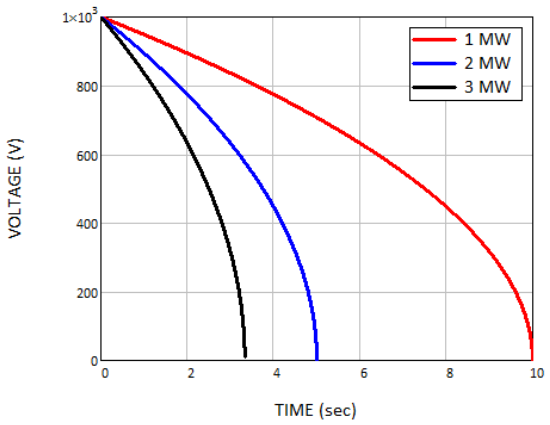

Fig. 1. Example of voltage decay for a 20-F, 1,000-V supercapacitor bank at three different discharging power levels

A similar equation can be derived for the charging process when the capacitor storage is being charged at a constant charging current:

$$V(t) = \frac{I}{C}t \qquad (5)$$

where I is the constant charging current. According to (5), the capacitor voltage will increase linearly until the maximum allowed voltage level is reached.

Fig. 2 shows an example of the voltage profiles for the same 20-F supercapacitor bank during constant current charging for three different charging currents: 1,000 A, 2,000 A, and 3,000 A.

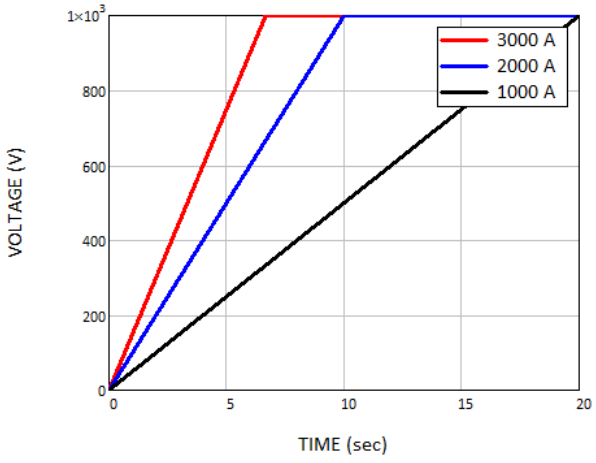

Fig. 2. Example of linear voltage rise for a 20-F, 1,000-V supercapacitor bank at three different charging currents

Of course, for such an operation, a power conversion system with the appropriate power rating would be necessary between the capacitor bank and the power grid, and it would be required to transfer bidirectional power flow so that the capacitor bank could be charged or discharged depending on the power system conditions. Bidirectional power flow can be accomplished by a current-bidirectional, *two-quadrant* switch network [11]. Fig. 3 shows the topology of the DC-DC converter using two transistor switches. A DC-DC converter interfaces supercapacitor storage to the main DC power bus of the storage system (a similar topology is used in the Bitrode converter at Idaho National Laboratory in their power-hardware-in-the-loop experimental setup for front-end controller testing). The bank of supercapacitors can be represented by its equivalent capacitance, C_{eq}, and resistance, R_{eq}, as shown in Fig. 3.

Transistors with anti-parallel diodes form current-bidirectional switches. Transistor T_2 is driven with the complement of the T_1 drive signal, such that T_2 is off when T_1 is on and vice versa. To charge the capacitor energy storage, the inductor current, $i_L(t)$, is positive and flows through transistor T_1 and diode D_2. To discharge the storage, the current, $i_L(t)$, reverses polarity and flows through transistor T_2 and diode D_1. In both cases, the capacitor bank voltage is less than the main DC bus voltage. The magnitude and polarity of the capacitor bank current can be controlled via adjustment of the duty cycle, D.

Switching loss imposes an upper limit on the switching frequencies of practical converters. During the switching transitions, the transistor voltage and current are simultaneously large. Consequently, the transistor experiences high instantaneous power loss. This can lead to significant average power loss, even though the switching transitions are short in duration. Switching loss causes the converter efficiency to decrease as the switching frequency is increased. The switching characteristic must be designed to ensure that the power electronic switches operate within the safe operating area as specified on the data sheet provided by the device manufacturer.

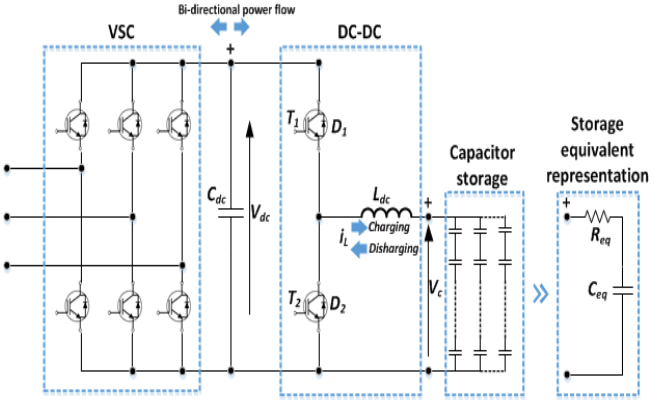

Fig. 3. Electric topology of supercapacitor energy storage

With the DC-DC converter topology shown in Fig. 3, two modes of operation are employed and three-phase voltage source converter maintains a constant DC bus voltage, V_{DC}.

The first mode is the charging mode at constant charging current, when the DC-DC converter operates in buck mode with output voltage V_c (under ideal conditions):

$$V_C = D \cdot V_{DC} \quad (6)$$

where D is the duty ratio of the pulse width modulation (PWM) gating applied to the switch T_1, and the switch T_2 is not gated at all.

In the second mode, the converter operates in boost mode, and the battery discharges to inject power into the load, and the output voltage of the DC-DC converter is given by:

$$V_{DC} = \frac{V_C}{1-D} \quad (7)$$

where D is the duty cycle of the PWM gating for switch T_2.

The inductive choke, L_{dc}, should be optimized for size, current ripple, minimum losses to avoid thermal runaway, and converter performance. Assuming constant capacitor voltage, V_c, the current ripple in the inductor can be calculated as:

$$\Delta I = \frac{V_{DC}}{f_{PWM} L_{dc}} D(1-D) \quad (8)$$

where, f_{PWM} is the PWM switching frequency of the power converter.

According to (8), the maximum current ripple, ΔI_{max}, will take place when $D = 0.5$. The current ripple should be as low as possible because it contributes to iron and copper losses, and it creates a vibration and audible noise (hum). It can be reduced if the DC-DC converter operates at low duty cycles and also by using higher switching frequencies and larger inductances.

The DC bus voltage ripple, ΔV_{DC}, can be reduced by choosing a size of the DC bus capacitor according to:

$$\Delta V_{DC} = \frac{D(1-D)V_C}{16 f_{PWM}^2 L_{dc} C_{eq}} \quad (9)$$

III. Control of Supercapacitor Energy Storage

The transient model of the supercapacitor system depicted in Fig. 3 has two interdependent controllers. The first controller is used for the voltage source inverter to ensure stable DC bus voltage and provide reactive power/voltage control on the AC side of the system. The second controller is for the DC-DC converter, and it provides constant voltage charge (buck mode) or constant power discharge (boost mode) mode for the supercapacitor energy storage depending on the grid conditions or set points from the grid energy management system.

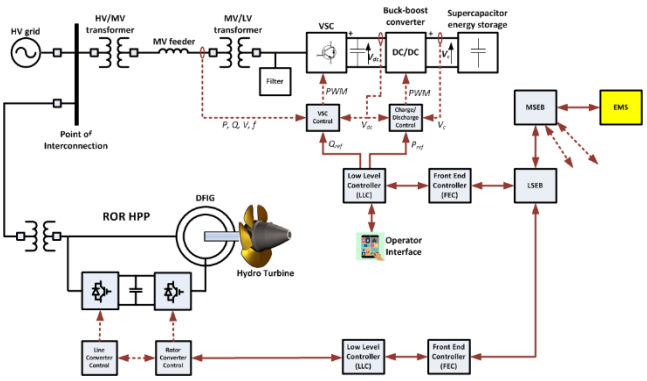

Fig. 4. Control of supercapacitor energy storage coupled with ROR-HPP

Fig. 4 shows the control diagram for the supercapacitor's energy storage in combination with a run-of-the-river (ROR), doubly-fed induction generator (DFIG)-based hydropower plant (HPP) coupled in coordinated control schemes using both low-level and supervisory controllers. The low-level supervisory controllers of the ROR HPP and supercapacitor energy storage systems are integrated into the overall power grid via agent-based front-end controllers that allow for the implementation of decentralized control. Local smart energy boxes (LSEB) make the dispatch decisions for each generating unit. A master smart energy box (MSEB) is installed at the system operator side, and it communicates the regional generation dispatch information from an energy management system.

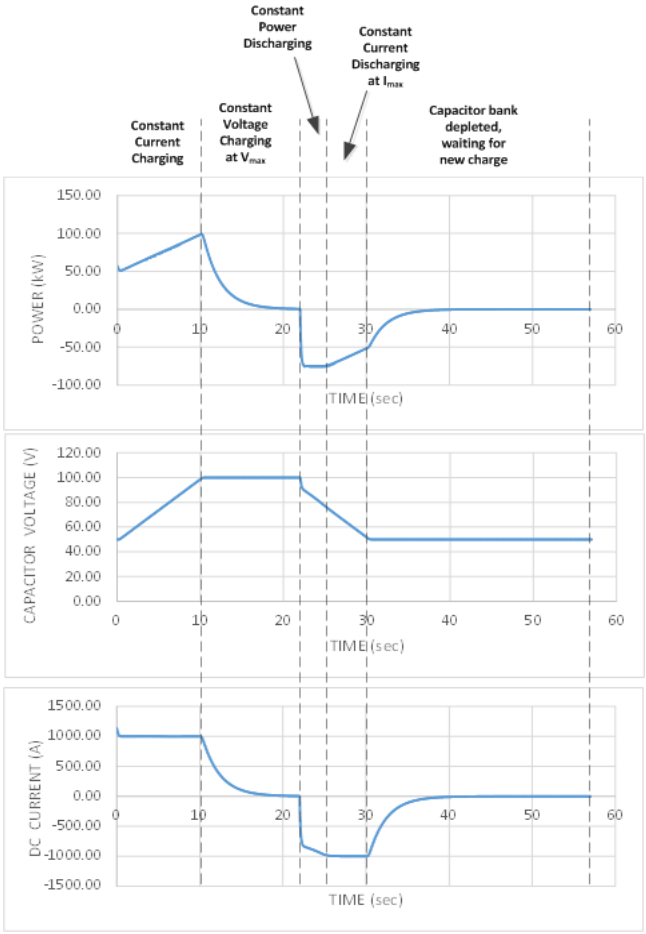

Fig. 5. Supercapacitor charging/discharging controls explained

The supercapacitor is charged or discharged by adjusting the voltage across the capacitor bank via duty-cycle control of the DC-DC converter. Fig. 5 demonstrates the operation of the supercapacitor energy storage using the results of a PSCAD simulation. The simulation was conducted on a 200-F capacitor storage model that operates at 100 V. Here we show the simulated averaged DC voltage, current, and power on capacitor storage terminals to demonstrate various charging/discharging modes for capacitor storage. First, the capacitor bank is charged using power from the grid at a constant DC charging current until the voltage across the capacitor bank reaches it maximum value of V_{max}.

After this, the charging is continued at reduced current to ensure that capacitor voltage does not exceed the safe limit. Next, the discharging power set point of 75 kW is sent by the front-end controllers and the capacitor storage discharges at that power level until the discharged DC current reaches its maximum level of I_{max}. At this point, constant current discharge continues until the capacitor voltage reaches its minimum value. From there, the capacitor bank is essentially depleted, waiting for a new charging/discharging cycle. The duration of the discharging period can be controlled by the value of the discharging power set point. In the above example, the capacitor storage was capable of delivering 75 kW for approximately 4 s and lower power during the rest of discharging process. Special control can be implemented to shape both the charging and discharging power profiles to provide maximum benefit to the system during normal and contingency conditions.

IV. System Coordination Control

To investigate the control coordination between the supercapacitor and other power plants, we use an IEEE 14-bus system. Fig. 6 shows the simplified IEEE 14-bus system connected to the 450-MW, ROR-DFIG hydropower plant (rated at 75 MW), and the 20-MW supercapacitor is added to the system. The total load is approximately 250 MW before the additional 35MW load connected to the grid at t=11s, to perturb the system. The dynamic simulations shown in this section were implemented using the PSCAD software platform [12].

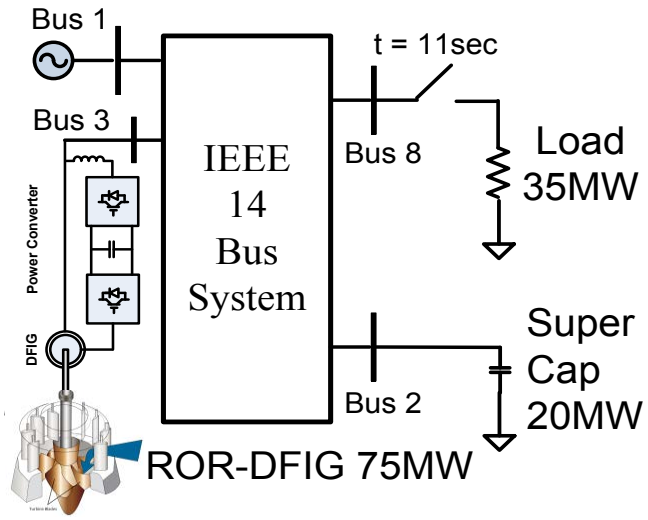

Fig. 6. Simplified diagram of the IEEE 14-bus system.

1. *Case I: Base Case—Gas Turbine Plant Provides Voltage and Frequency Regulation.*

In the base case of operation, we simulate a gas turbine power plant at Bus 1 providing both the frequency regulation via its governor and the voltage regulation via its exciter. Initially, the gas turbine power plant is operated at 250 MW to supply the loads in the system. The ROR-DFIG power plant is then commanded to deliver a reference power of 45 MW. The gas turbine is operated with a governor with droop control. The additional 35-MW load is connected at t = 11 s and disconnected at t = 25 s. Fig. 7 shows the output of the gas turbine power plant. Detailed discussions on DFIG for hydropower plant can be found in references [13-16].

Originally, the steady-state frequency measured at t = 10 s is at f = 0.9975p.u. In response to the load insertion, the grid frequency suddenly drops to f = 0.9925 p.u. The output power of the gas turbine rises as the droop controller adjusts the output power based on the frequency deviation (see Fig. 7b). The output power finally settles when the frequency reaches a new steady state. Similarly, when the 35-MW load is again disconnected from the grid, the frequency of the grid returns to the original value, and the output power of the gas turbine returns to its original value.

The grid voltage as shown in Fig. 7c is well regulated by the exciter of the gas turbine. No significant changes or fluctuations of the reactive power generated by the gas turbine occur when the load is disconnected from the grid or when the load is reconnected to the grid.

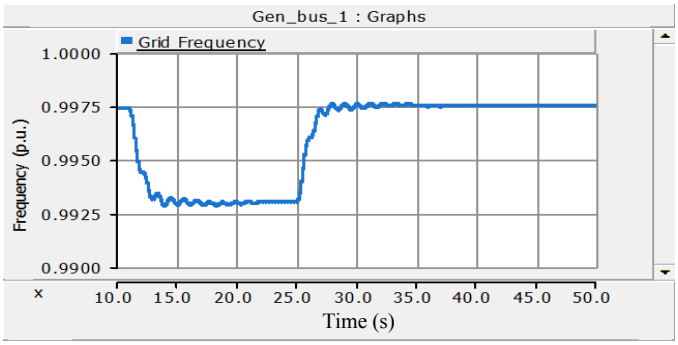

(a) Frequency

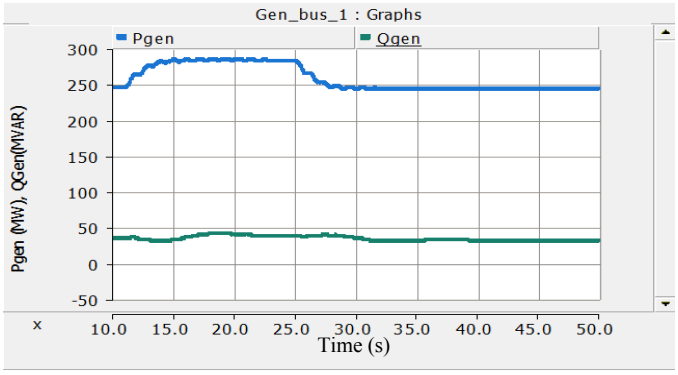

(b) Output real and reactive power

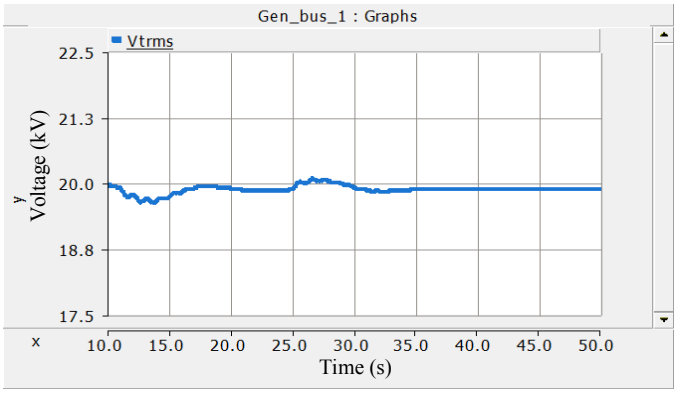

(c) Terminal voltage

Fig. 7. Time series of the gas turbine output for the base case scenario

As shown in Fig. 8, the ROR-DFIG HPP delivers a constant output power and does not contribute to frequency regulation. The output power of the ROR-DFIG is set at 45 MW. The ROR-DFIG HPP is not set to control the output voltage, and the reactive power output is set to zero.

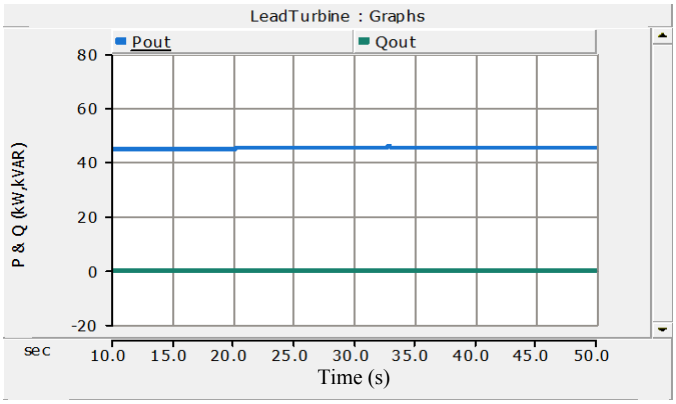

Fig. 8. Real and reactive power output of the ROR-DFIG HPP for the base case scenario

2. *Case II: Gas Turbine and ROR-DFIG Share Frequency Regulation with Droop Control*

In Case II, the gas turbine power plant and the ROR-DFIG share frequency regulation (both with droop control) and the same sequence of load insertion and removal is repeated. Fig. 9 shows the grid frequency throughout this scenario. A significant improvement is achieved relative to the base case as the grid frequency settles at f = 0.995 p.u.

Fig. 10 shows the real and reactive power of the ROR-DFIG. The ROR-DFIG is controlled to generate at unity power factor. When the frequency dips because of the load increase (35 MW), both the gas turbine and the ROR-DFIG share the burden of regulating the frequency via droop control. Similarly, during the load disconnection, when the frequency rises, the droop control of the gas turbine and the ROR-DFIG share regulating the frequency. As shown in Fig.10, the output power increases to 68 MW before returning to 45 MW when the load is disconnected from the grid. The frequency finally settles at f =0.9975 p.u. Because both the gas turbine and the ROR-DFIG share the burden of frequency regulation, the minimum frequency during the dip is at f = 0.9950 p.u., whereas f = 0.9930 p.u. in the base case (Fig. 7a).

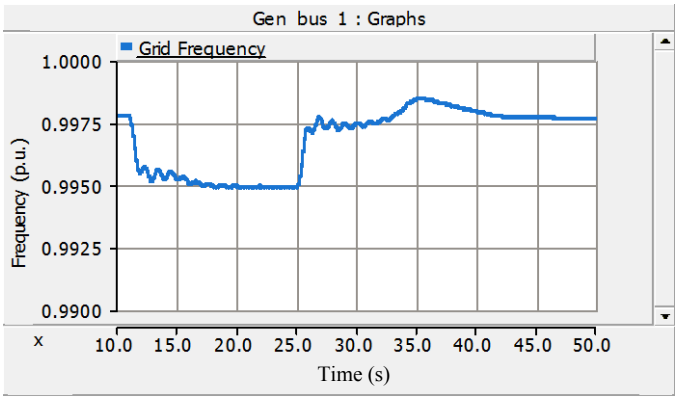

Fig. 9. Grid frequency for Case II

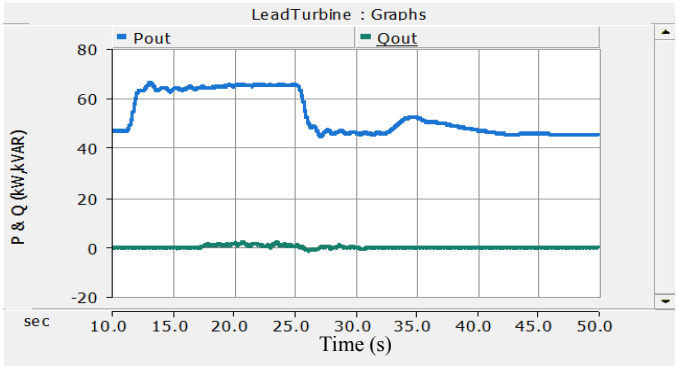

Fig. 10. Real and reactive power output of the ROR-DFIG HPP for Case II

3. *Case III: Gas Turbine Is Controlled with Droop, Supercapacitor Provides Inertial Response*

In Case III, the gas turbine power plant provides frequency regulation, the supercapacitor provides inertial response, and the ROR-DFIG output is kept at 45 MW constant output power (as in Case I).

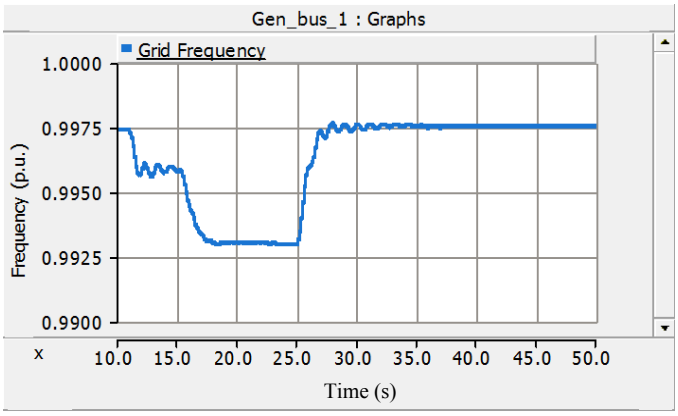

Fig. 11. Grid frequency for Case III with supercapacitor providing inertial response to the grid

The supercapacitor is a very good short-term energy storage solution to supply surges of power to the grid when needed. Thus, its energy content does not need to be large, but it can be sized for short durations.

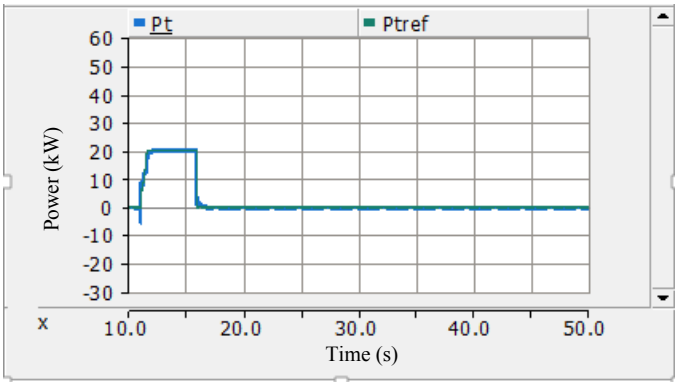

Fig. 12. Real power output of the supercapacitor for Case III

As shown in Fig. 11, initially the grid frequency drops when the 35-MW load is connected to the grid at t = 11 s. The grid frequency is affected by the contribution of the supercapacitor at t = 11 s, and the grid frequency can be brought up to more than f = 0.9950 p.u. for a short duration. The frequency drops again when the contribution of the supercapacitor diminishes when the minimum charge has been reached. The frequency of the grid returns to normal when the load is disconnected from the grid. Fig. 12 shows that the output power of the supercapacitor lasts for only 5 s.

4. *Case IV: Gas Turbine and ROR-DFIG Are Controlled with Droop, Supercapacitor Provides Inertial Response*

In Case IV, the gas turbine power plant and ROR-DFIG provide the frequency regulation, and the supercapacitor provides inertial response. This is a combination of Case II and Case III.

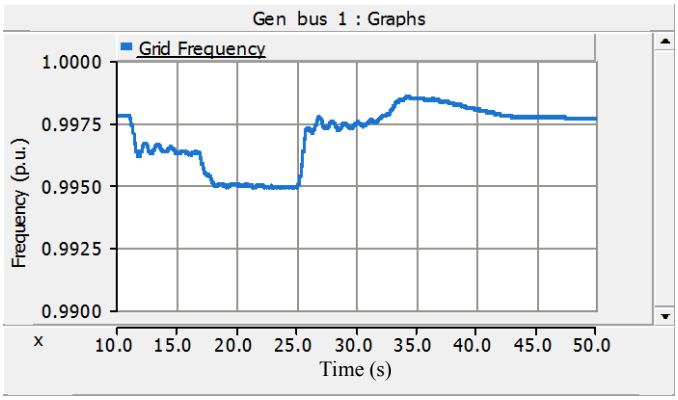

Fig. 13. Grid frequency for Case IV

As shown in Fig. 13, when the first occurrence of the frequency drop is detected, the supercapacitor is deployed; at the same time, both the gas turbine and the ROR-DFIG provide the frequency regulation via governor action and the frequency dips to f = 0.9960 p.u. When the supercapacitor reaches the minimum amount of energy stored, it is disconnected from the grid, and the frequency drops further, down to f = 0.9950 p.u. Note, there is sluggishness of the gate of the hydropower in controlling the rotational speed that causing the frequency deviation (up) around t=35s.

Comparing Fig. 14 to Fig. 7b shows that the burden of carrying the additional load has been significantly reduced for the gas turbine as the ROR-DFIG increases its output with the frequency decline (droop action).

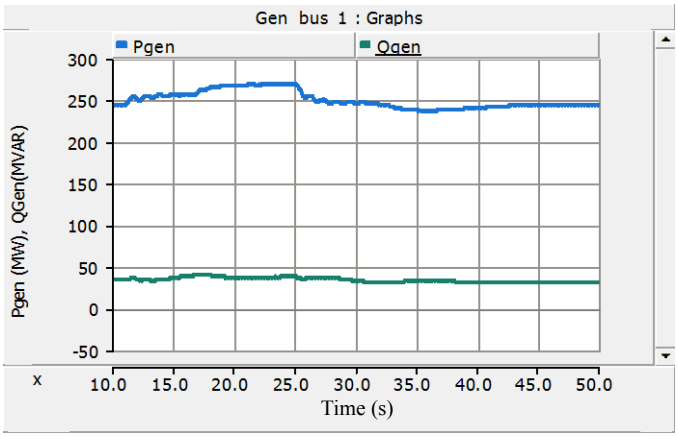

Fig. 14. Real and reactive power of the gas turbine for Case IV

5. *Case V: ROR-DFIG Is Controlled with Droop with Automatic Generation Control Functionality*

In case II and IV, the ROR-DFIG is deployed so that it and the gas turbine provide frequency regulation, and the supercapacitor provides inertial response. In Case V, we include the AGC action from the ROR-DFIG to tighten the frequency regulation.

Fig. 15 shows that the grid frequency is tightly controlled with support from the ROR-DFIG. Note that the power converter allows for quick response in delivering real power from the power plant because it is not limited by the sluggish mechanical response time. The frequency is maintained within close proximity to f = 0.9980 p.u. throughout the window of observation.

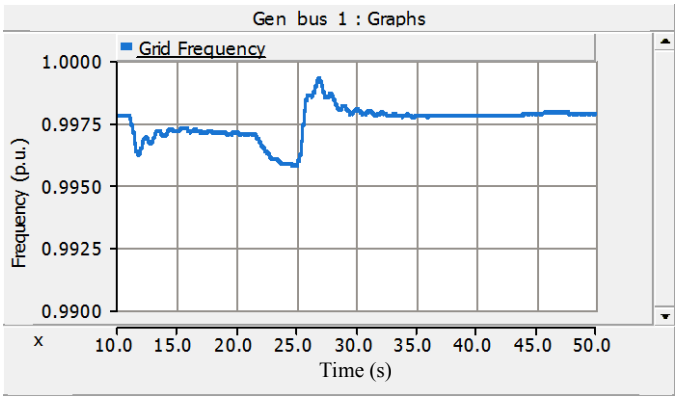

Fig. 15. Grid frequency for case V

Fig. 16 shows the output real and reactive power of the ROR-DFIG. Here, the power rating of the ROR-DFIG (75 MW) has been reached during the transient between the load connection and disconnection from the grid. The reactive power stays at a minimum because the ROR-DFIG is controlled at unity power factor. As shown in Figure 15, the role of the supercapacitor is to provide fast, short-term support in the form of additional inertial response to the grid. The gas turbine and the ROR-DFIG provide the governor response and the ROR-DFIG also provides the AGC in the longer term.

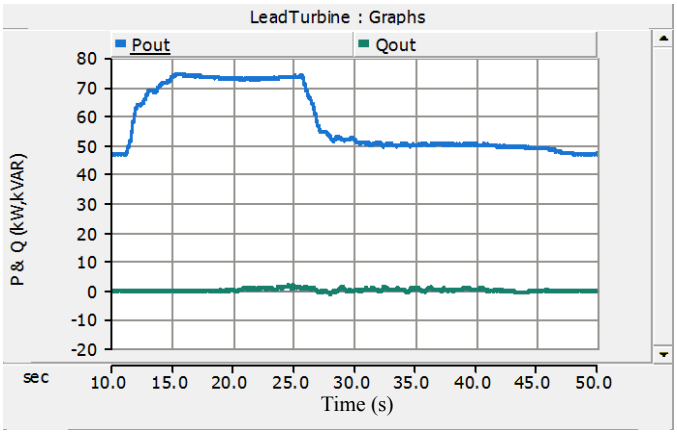

Fig. 16. Real and reactive power of the ROR-DFIG for Case V

Note, that the ROR-DFIG reaches its maximum power rating (75MW), and cannot provide additional power. The super capacitor is operated at unity power factor; Fig. 17 shows the corresponding output real power of the supercapacitor.

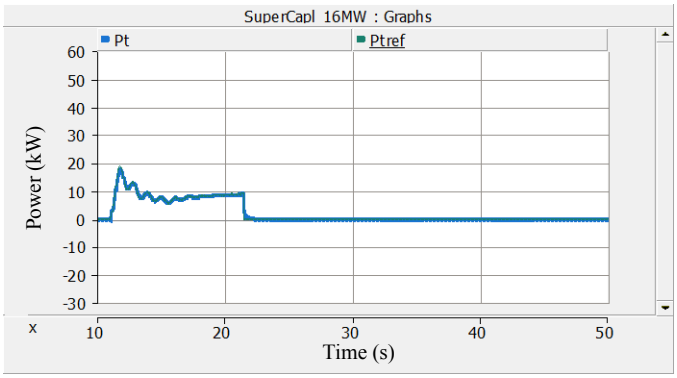

Fig. 17. Real power output of supercapacitor for Case V

V. Conclusions

The work presented in this paper includes the development of an electromagnetic transient model of a supercapacitor and a dynamic simulation of a supercapacitor within the IEEE 14-bus test system that includes a gas turbine power plant, ROR-DFIG HPP. The development of the model components and functionalities include:

- Development of a supercapacitor dynamic model and demonstration of its capability to improve the power system stability and frequency regulation (virtual inertial response) for the first few seconds of a frequency dip
- Development of control coordination strategies among the gas turbine, ROR-DFIG, and supercapacitor
- Demonstrating the unique characteristics of ROR-DFIG to provide quick response and independent control of real and reactive power control
- Demonstrating the priority to support inertial response using short-term energy storage such as supercapacitors and to

support frequency regulation and automatic generation control using medium-fast generation such as ROR-DFIG

• Testing these dynamic models and control coordination strategies using a power system model based on the IEEE 14-bus test system using multiple scenarios. The exercise can be expanded to include optimum placement of various energy storage, or symmetrical and unsymmetrical faults at different buses.

VI. Acknowledgment

This work was supported by the U.S. Department of Energy under Contract No. DE-AC36-08-GO28308 with the National Renewable Energy Laboratory (NREL). The U.S. Government retains and the publisher, by accepting the article for publication, acknowledges that the U.S. Government retains a nonexclusive, paid-up, irrevocable, worldwide license to publish or reproduce the published form of this work, or allow others to do so, for U.S. Government purposes. This work is a collaborative work among NREL, Idaho National Laboratory, and Argonne National Laboratory.

VII. References

[1] S. Salinas, M. Li, P. Li, and Y. Fu, "Dynamic energy management for the smart grid with distributed energy resources," IEEE Trans. Smart Grid, vol. 4, no. 4, pp. 2139–2151, Dec 2013.

[2] L. L. Lai and T. F. Chan, Distributed generation: Induction and permanent magnet generators. John Wiley & Sons, 2008.

[3] F. Katiraei, R. Iravani, N. Hatziargyriou, and A. Dimeas, "Microgrids management," IEEE Power and Energy Magazine., vol. 6, no. 3, pp. 54–65, May 2008.

[4] J. Zhao, K. Graves, C. Wang, G. Liao, and C.-P. Yeh, "A hybrid electric/hydro storage solution for standalone photovoltaic applications in remote areas," in Proc. IEEE Power and Energy Society General Meeting, San Diego, CA, 2012, pp. 1–6.

[5] J. Barton and D. Infield, "Energy storage and its use with intermittent renewable energy," IEEE Trans. Energy Conversion, vol. 19, no. 2, pp. 441–448, June 2004.

[6] M. Molina, "Distributed energy storage systems for applications in future smart grids," in Proc. 6th IEEE/PES Transmission and Distribution. Latin Amer. Conf. Exposit., Sept 2012, pp. 1–7.

[7] J. W. Shim, Y. Cho, S.-J. Kim, S. W. Min, and K. Hur, "Synergistic control of smes and battery energy storage for enabling dispatchability of renewable energy sources," IEEE Trans. Applied Superconductivity, vol. 23, no. 3, pp. 5 701 205–5 701 205, June 2013.

[8] V. Boicea, "Energy storage technologies: The past and the present," Proc. IEEE, vol. 102, no. 11, pp. 1777–1794, Nov 2014.

[9] I. Miranda, N. Silva, and A. Maia Bernardo, "Assessment of the potential of battery energy storage systems in current European markets designs," in Proc. International Conference on the European Energy Market (EEM), May 2015, pp. 1–5.

[10] M. Winter and R. J. Brodd, "What are batteries, fuel cells, and supercapacitors?" Chemical reviews, vol. 104, no. 10, pp. 4245–4270, 2004.

[11] X. del Toro Garcia, P. Roncero-Sanchez, A. Parreno, V. Feliu, "Ultracapacitor-based Storage: Modeling, Power Conversion and Energy Considerations", IEEE 2010 International Symposium on Industrial Electronics.

[12] PSCAD™/EMTDC™, https://hvdc.ca/pscad/

[13] E. Muljadi, M. Singh, V. Gevorgian, M. Mohanpurkar, R. Hovsapian, and V. Koritarov, "Dynamic Modeling of Adjustable-Speed Pumped Storage Hydropower Plant," presented at the IEEE Power and Energy Society General Meeting, Denver, Colorado, July 26 – 30, 2015

[14] V. Koritarov, L. Guzowski, J. Feltes, Y. Kazachkov, B. Gong, B. Trouille, and P. Donalek, "Modeling adjustable speed pumped storage hydro units employing doubly-fed induction machines," Argonne National Laboratory, Lemont, IL, Tech. Rep. ANL/DIS-13/06, Aug. 2013.

[15] J. Janning and A. Schwery, "Next generation variable speed pump-storage power stations," presented at EPE 2009, the 13th European Conference on Power Electronics and Applications, Barcelona, Spain, 2009.

[16] V. Koritarov, J. Feltes, Y. Kazachkov, B. Gong, P. Donalek, and V. Gevorgian, "Testing dynamic simulation models for different types of advanced pumped storage hydro units," Argonne National Laboratory, Lemont, IL, Tech. Rep. ANL/DIS-13/08, Aug. 2013.